

Supporting Information

Reversible and topotactic solvent removal in magnetic Ni(NCS)₂ coordination polymer

Stefan Suckert,[†] Michał Rams,[‡] Marek M. Rams,[‡] and Christian Näther^{,†}*

[†] Institut für Anorganische Chemie, Christian-Albrechts-Universität zu Kiel, Max-Eyth-Straße 2, 24118 Kiel, Germany. cnaether@ac.uni-kiel.de

[‡] Institute of Physics, Jagiellonian University, Łojasiewicza 11, 30-348 Kraków, Poland.

Content

Tab. S1	Selected crystal data and details of the structure refinements.	3
Fig. S1	IR spectra of 1 -MeCN.	4
Fig. S2	DTA, TG and DTG curve for 1 -MeCN at 4 °C/min.	4
Fig. S3	Experimental and calculated XRPD pattern for 1 -MeCN.	5
Fig. S4	ORTEP plot of 1 -MeCN.	5
Tab. S2	Selected bond lengths and angles for 1 -MeCN.	6
Fig. S5	Calculated XRPD pattern of 1 -MeCN with and without the acetonitrile solvent molecules.	6
Tab. S3	Selected hkl indices and calculated as well as measured intensities for reflections with $h+k = 2n+1$ (left) and $h + k = 2n$ (right) for 1 .	6
Fig. S6	DTA, TG and DTG curve for 1 -MeCN at 1°C/min.	7
Fig. S7	Experimental XRPD pattern of the residue formed after acetonitrile removal by thermogravimetric measurements and powder pattern of 1 -MeCN calculated without and with acetonitrile.	7
Fig. S8	IR spectra of 1 -MeCN and 1 .	8
Fig. S9.	Experimental XRPD pattern of the residue formed after the second TG step in the thermogravimetric measurement of 1 -MeCN and XRPD pattern of 1 -MeCN calculated from the single crystal structure.	8
Fig. S10	Temperature-dependent XRPD measurements of 1 -MeCN.	9
Fig. S11	Experimental XRPD pattern of the residue obtained by storing 1 -MeCN in vacuum and of the residue formed after acetonitrile removal by thermogravimetric measurements and powder pattern of 1 -MeCN calculated from the single crystal structure (bottom).	9
Fig. S12	Time-dependent XRPD patterns of 1 -MeCN on storage at room-temperature.	10

Fig. S13	DTA-TG curve of 1 stored in an acetonitrile atmosphere for several hours.	11
Fig. S14	Experimental XRPD pattern of 1 and XRPD patterns of 1 after one night in water and ethanol atmosphere as well as 1 h at a methanol atmosphere.	11
Fig. S15	Reciprocal space plots for 1 -MeCN and 1 -MeCN-A.	12
Fig. S16	Reciprocal space plots for 1 -MeCN-B and 1 -MeCN-C.	13
Fig. S17	Reciprocal space plots for 1 -MeCN-D and 1 -MeCN-E.	14
Fig. S18	Reciprocal space plots for 1 and 1 -MeCN-re.	15
Fig. S19	Unit cell and void volume as function of the number of electrons within the voids and the sof.	16
Fig. S20	Length of the crystallographic <i>a</i> -, <i>b</i> - and <i>c</i> -axis as function of the number of electrons within the voids and the sof of the acetonitrile molecules.	17
Tab. S4	Comparison of selected bond lengths and angles for 1 -MeCN and 1 .	18
Fig. S21	Microscopic images of selected crystals of 1 -MeCN, after removal of solvent and after storage in a saturated acetonitrile atmosphere.	19
Fig. S22	Experimental XRPD pattern of 1 after sorption measurements and calculated pattern of 1 .	20
Fig. S23	Magnetic susceptibility measured at 30 Oe for 1 -MeCN, 1 and 1 ds.	20
Fig. S24	Field dependence of magnetization measured for 1 -MeCN and 1 .	21
Fig. S25	Comparison of two methods used to calculate the susceptibility for a powder sample	21
Fig. S26	Magnetic susceptibility χ (powder average, shown χT product) calculated with DMRG method for the Heisenberg chain of spins $S = 1$ for different exchange interaction J and fixed zero-field splitting parameter D and fixed factor $g = 2.2$.	22
Fig. S27	Specific heat C of the Heisenberg chain of spins $S = 1$ with fixed exchange interaction J and different zero-field splitting parameters D in zero field $H = 0$ calculated using the DMRG method.	22
	Comments on checkcif reports	23

Table S1. Selected crystal data and details of the structure refinements. Please note, that for the experiments on solvent removal three different single crystals were used. ^a These values originates from a removal of the solvent molecules using the Squeeze option in Platon. **1-re** corresponds to the crystal obtained by storing **1** in an MeCN atmosphere.

compound	1-MeCN	1-MeCN-A	1-MeCN-B	1-MeCN-C
formula	C ₂₄ H ₃₁ NiN ₇ O ₄ S ₂	C _{23.53} H _{30.30} N _{6.77} NiO ₄ S ₂	C _{23.65} H _{29.95} N _{6.65} NiO ₄ S ₂	C _{23.45} H _{29.36} N _{6.45} NiO ₄ S ₂
MW / g mol ⁻¹	604.39	597.13	594.29	588.55
sof MeCN	1	0.768(8)	0.651(7)	0.455(8)
No. of electrons	81 ^a	72 ^a	54 ^a	48
crystal system	monoclinic	monoclinic	monoclinic	monoclinic
space group	P2 ₁ /c	P2 ₁ /c	P2 ₁ /c	P2 ₁ /c
<i>a</i> / Å	26.5715(7)	26.5985(11)	26.6240(7)	26.6565(8)
<i>b</i> / Å	11.4534(4)	11.4276(6)	11.4168(4)	11.3970(5)
<i>c</i> / Å	9.8286(2)	9.8235(2)	9.8167(3)	9.8139(3)
<i>a</i> / °	90	90	90	90
<i>β</i> / °	94.982(2)	94.932(3)	95.053(2)	95.123(3)
<i>γ</i> / °	90	90	90	90
<i>V</i> / Å ³	2979.9(2)	2974.9(2)	2972.3(2)	2969.6(2)
<i>T</i> / K	200(2)	200(2)	200(2)	200(2)
<i>Z</i>	4	4	4	4
<i>D</i> _{calc} / g cm ⁻³	1.347	1.328	1.328	1.316
<i>μ</i> / mm ⁻¹	0.832	0.832	0.83	0.832
<i>θ</i> _{max} / deg	25.499	25.242	25.497	25.498
measured refl.	22963	25191	25093	24665
unique refl.	5511	5509	5502	5486
refl. <i>F</i> ₀ >4σ(<i>F</i> ₀)	4474	3985	4135	3824
parameter	345	345	345	346
<i>R</i> _{int}	0.0729	0.1522	0.0827	0.1060
<i>R</i> ₁ [<i>F</i> ₀ > 4σ(<i>F</i> ₀)]	0.0421	0.0613	0.0486	0.0540
<i>wR</i> ₂ [all data]	0.1251	0.1935	0.1563	0.1808
GOF	1.030	1.051	1.080	1.072
Δρ _{max/min} / e Å ⁻³	0.483/ -0.590	0.586/ -0.848	0.395/ -0.891	0.429/ -0.839

compound	1-MeCN-D	1-MeCN-E	1	1-re
formula	C ₂₂ H ₂₈ NiN ₆ O ₄ S ₂	C ₂₂ H ₂₈ NiN ₆ O ₄ S ₂	C ₂₄ H ₃₁ NiN ₇ O ₄ S ₂	C _{23.92} H _{30.88} NiN _{6.96} O ₄ S ₂
MW / g mol ⁻¹	563.33	563.33	563.33	602.78
sof MeCN	-	-	-	0.960(8)
No. of electrons	25	14	8	88
crystal system	monoclinic	monoclinic	monoclinic	monoclinic
space group	C2/c	C2/c	C2/c	P2 ₁ /c
<i>a</i> / Å	26.7203(10)	26.7293(10)	26.7251(8)	26.5828(10)
<i>b</i> / Å	11.3765(6)	11.3512(6)	11.3245(5)	11.4485(5)
<i>c</i> / Å	9.8065(4)	9.8041(4)	9.8036(3)	9.8199(4)
<i>a</i> / °	90	90	90	90
<i>β</i> / °	95.453(3)	95.214(3)	94.922(2)	95.016(3)
<i>γ</i> / °	90	90	90	90
<i>V</i> / Å ³	2967.5(2)	2962.4(2)	2956.1(2)	2977.1(2)
<i>T</i> / K	200(2)	200(2)	200(2)	200(2)
<i>Z</i>	4	4	4	4
<i>D</i> _{calc} / g cm ⁻³	1.261	1.263	1.266	1.345
<i>μ</i> / mm ⁻¹	0.829	0.831	0.832	0.832
<i>θ</i> _{max} / deg	25.498	25.497	25.498	26.004
measured refl.	12482	12527	12694	22491
unique refl.	2748	2750	2743	5803
refl. <i>F</i> ₀ >4σ(<i>F</i> ₀)	2574	2555	2558	4487
parameter	163	164	163	346
<i>R</i> _{int}	0.0825	0.0663	0.0532	0.1156
<i>R</i> ₁ [<i>F</i> ₀ > 4σ(<i>F</i> ₀)]	0.0452	0.0458	0.0337	0.0666
<i>wR</i> ₂ [all data]	0.1223	0.1318	0.0967	0.1944
GOF	1.063	1.200	1.053	1.048
Δρ _{max/min} / e Å ⁻³	0.446/ -0.687	1.060/ -0.520	0.361/ -0.342	0.625/ -0.952

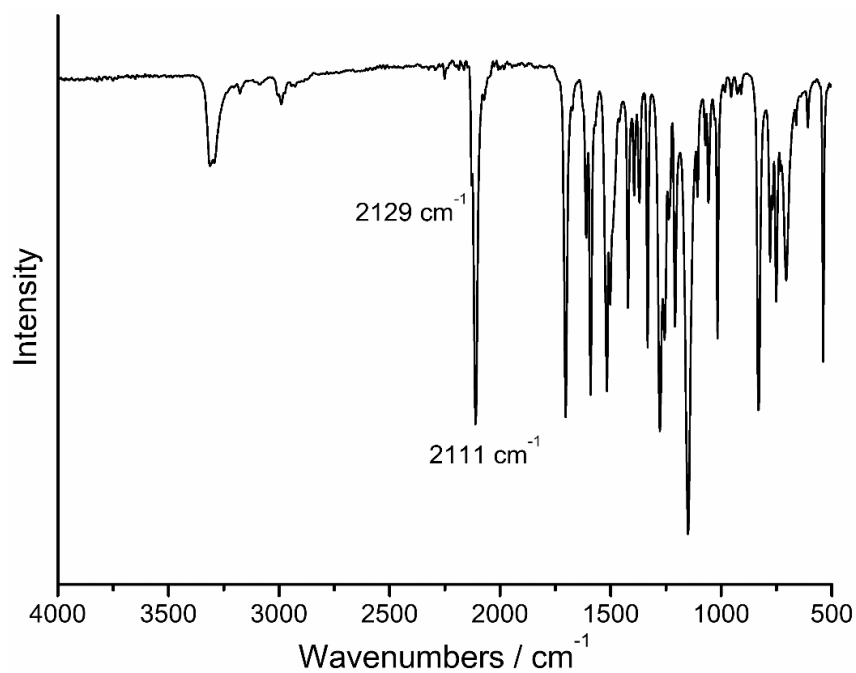


Figure S1. IR spectra of **1-MeCN**. Given are the values for the CN stretching vibration of the thiocyanate anion.

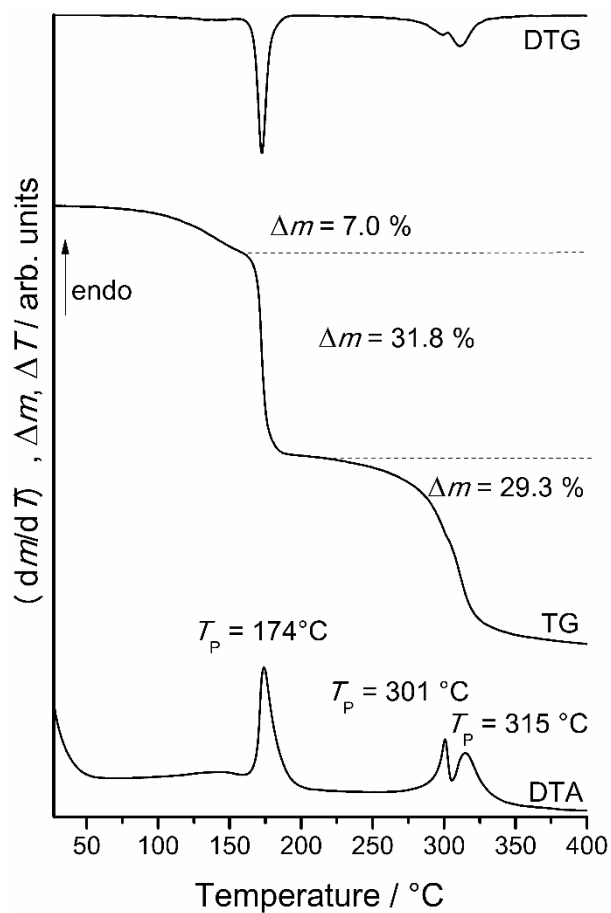


Figure S2. DTA, TG and DTG curve for **1-MeCN** at 4 °C/min.

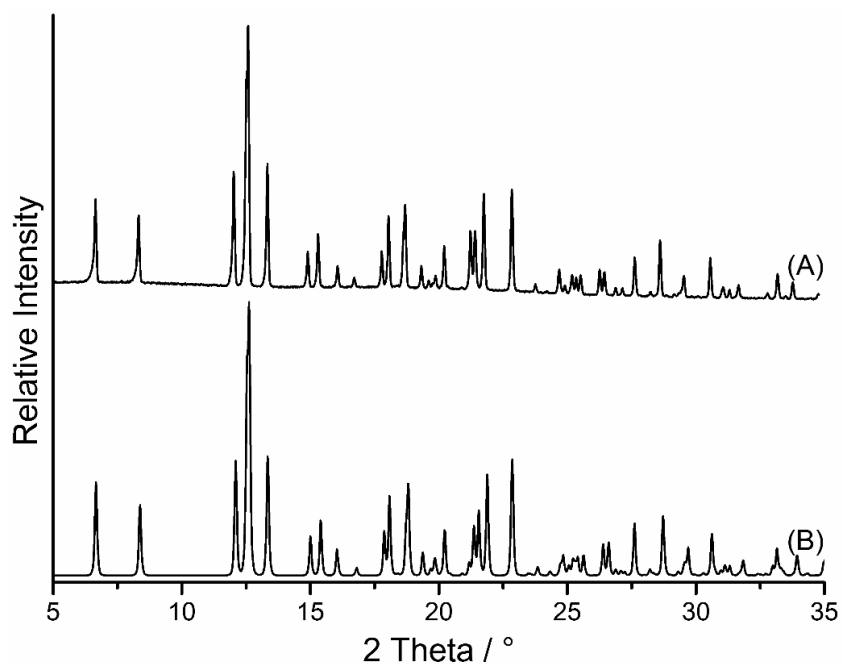


Figure S3. Experimental (A) and calculated (B) XRPD pattern for **1-MeCN**.

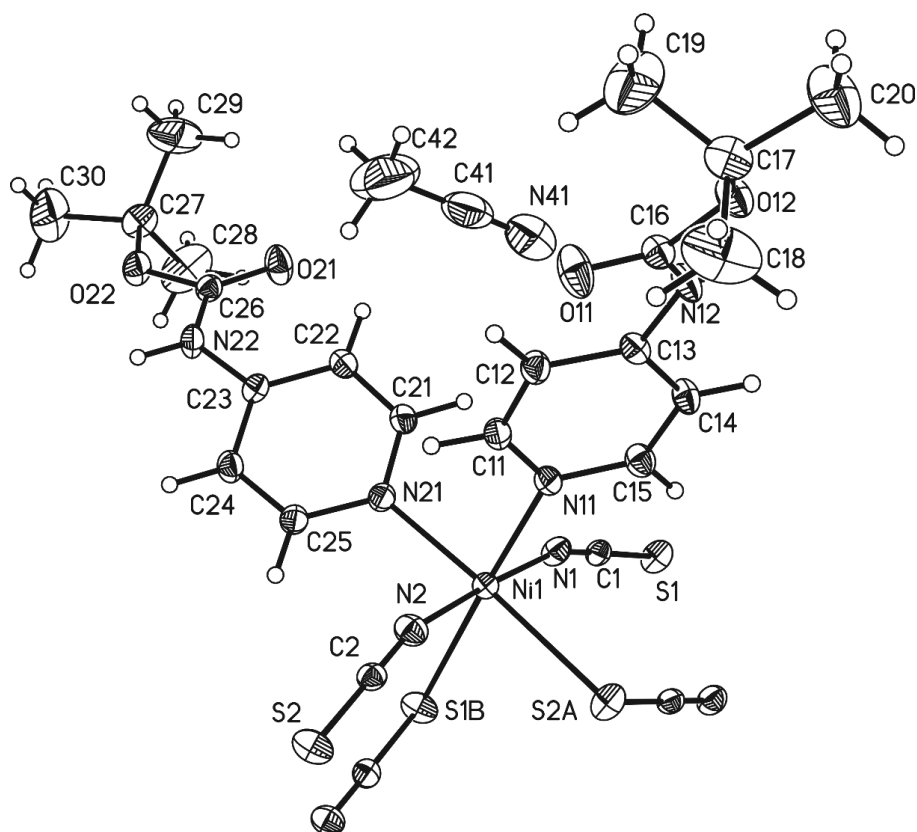
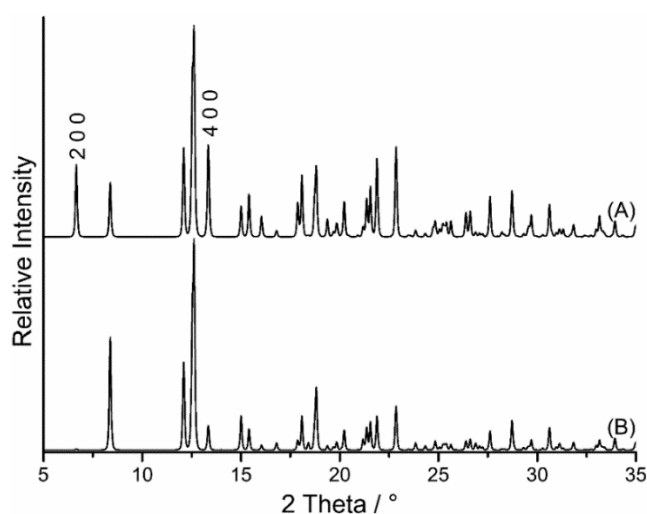


Figure S4. ORTEP plot of **1-MeCN** with labeling and displacement ellipsoids drawn at 50 % probability level. Symmetry codes: A = x, -y+3/2, z+1/2, .B = x, -y+3/2, z-1/2.

Table S2. Selected bond lengths and angles for **1**-MeCN.

Ni(1)-N(2)	2.0306(17)	Ni(1)-N(21)	2.0986(16)
Ni(1)-N(1)	2.0334(17)	Ni(1)-S(2)#1	2.5417(5)
Ni(1)-N(11)	2.0968(16)	Ni(1)-S(1)#2	2.5595(5)
N(2)-Ni(1)-N(11)	90.33(6)	N(11)-Ni(1)-S(2)#1	90.48(4)
N(1)-Ni(1)-N(11)	92.05(6)	N(2)-Ni(1)-S(1)#2	92.08(4)
N(2)-Ni(1)-N(21)	91.44(6)	N(1)-Ni(1)-S(1)#2	85.50(5)
N(1)-Ni(1)-N(21)	90.53(6)	N(21)-Ni(1)-S(1)#2	90.36(5)
N(11)-Ni(1)-N(21)	90.86(7)	S(2)#1-Ni(1)-S(1)#2	88.45(2)
N(2)-Ni(1)-S(2)#1	85.25(5)	N(11)-Ni(1)-S(1)#2	177.28(4)
N(1)-Ni(1)-S(2)#1	92.72(4)	N(21)-Ni(1)-S(2)#1	176.44(4)
N(2)-Ni(1)-N(1)	176.89(7)		

**Figure S5.** Calculated XRPD pattern of **1**-MeCN with (A) and without (B) the acetonitrile solvent molecules. The hkl indices of the two reflections showing the strongest changes is given.**Table S3.** Calculated as well as measured intensities for selected reflections with $h+k = 2n+1$ (left) and $h + k = 2n$ (right) for **1**.

h	k	l	I_{calc}	I_{obs}	h	k	l	I_{calc}	I_{obs}
5	0	0	27.72	-182.30	6	0	0	1046.23	974.43
7	0	0	94.07	52.24	8	0	0	7958.78	7310.14
9	0	0	97.93	101.33	10	0	0	3453.96	3153.58
11	0	0	147.23	123.61	12	0	0	4353.72	3917.28
13	0	0	11.94	-12.47	14	0	0	3455.90	3233.90
15	0	0	40.38	-35.47	16	0	0	49443.01	50803.42
17	0	0	57.31	40.20	18	0	0	6352.76	6318.28
19	0	0	5.12	-3.91	20	0	0	2990.86	3238.23
21	0	0	42.41	40.48	22	0	0	198.97	212.78
23	0	0	8.27	30.18	24	0	0	293.86	316.40
25	0	0	26.96	12.62	26	0	0	395.60	449.37
27	0	0	7.15	2.03	28	0	0	2609.42	2825.58
29	0	0	16.06	61.03	30	0	0	4551.02	4616.64
31	0	0	2.31	26.65	32	0	0	2280.46	2170.95
4	1	0	25.73	24.41	5	1	0	1313.27	1175.16
6	1	0	68.27	67.29	7	1	0	4269.82	3856.08
8	1	0	3.36	-9.33	9	1	0	7120.64	7008.30
10	1	0	140.43	119.25	11	1	0	1202.42	1340.38

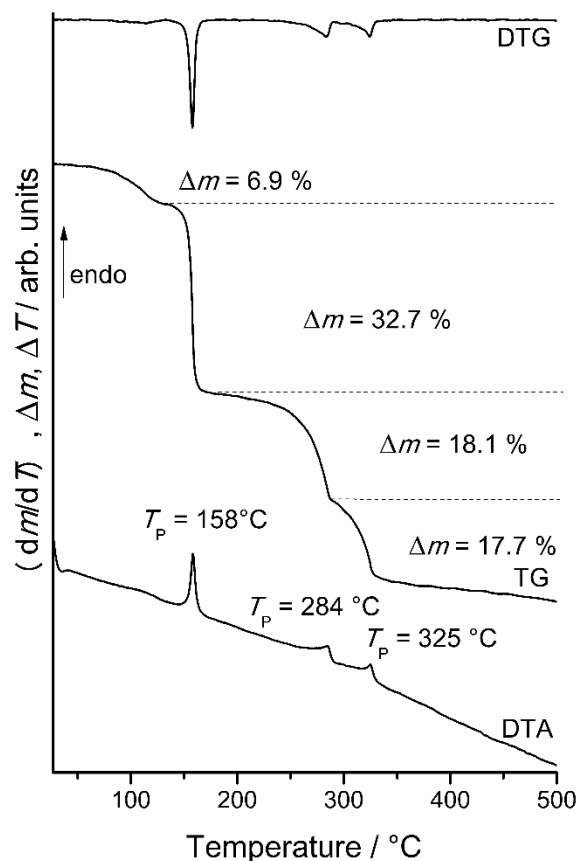


Figure S6. DTA, TG and DTG curve for **1-MeCN** at 1°C/min.

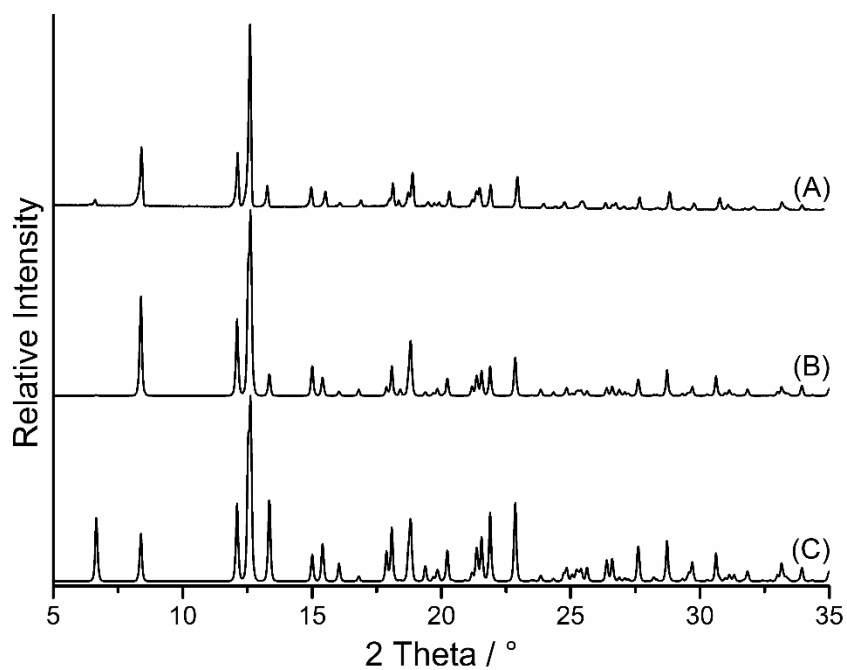


Figure S7. Experimental XRPD pattern of the residue formed after acetonitrile removal by thermogravimetric measurements (top), and powder pattern of **1-MeCN** calculated without (mid) and with acetonitrile (bottom).

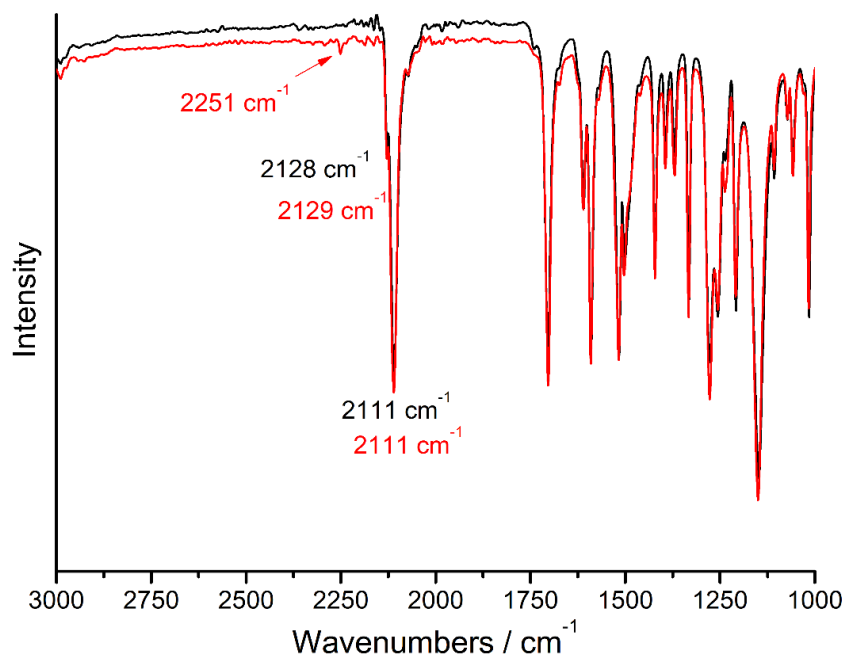


Figure S8. IR spectra of **1-MeCN** (red) and **1** (black).

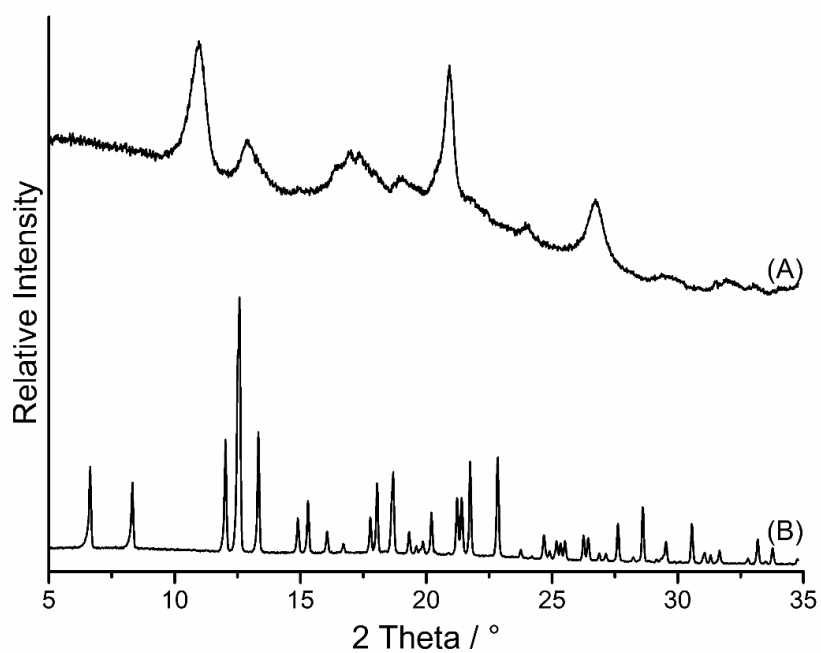


Figure S9. Experimental XRPD pattern of the residue formed after the second TG step in the thermogravimetric measurement of **1-MeCN** (A) and XRPD pattern of **1-MeCN** calculated from the single crystal structure (B).

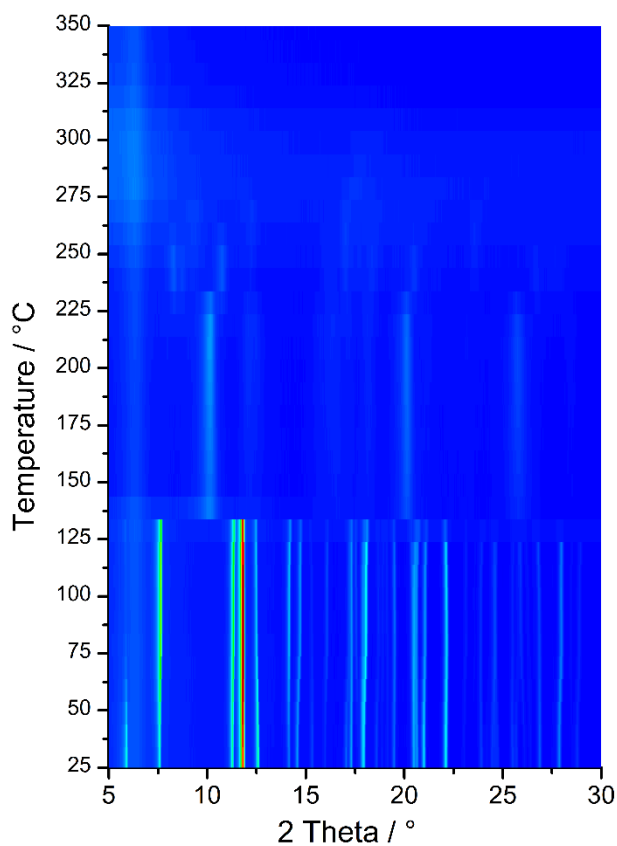


Figure S10. Temperature-dependent XRPD measurements **1-MeCN**.

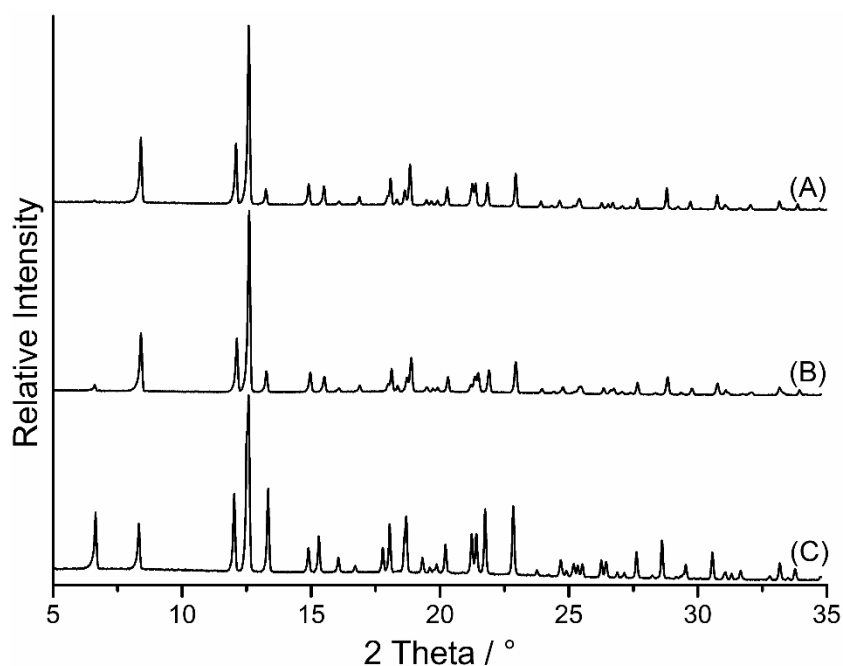


Figure S11. Experimental XRPD pattern of the residue obtained by storing **1-MeCN** in vacuum (A) and of the residue formed after acetonitrile removal by thermogravimetric measurements (B) and powder pattern of **1-MeCN** calculated from the single crystal structure (C).

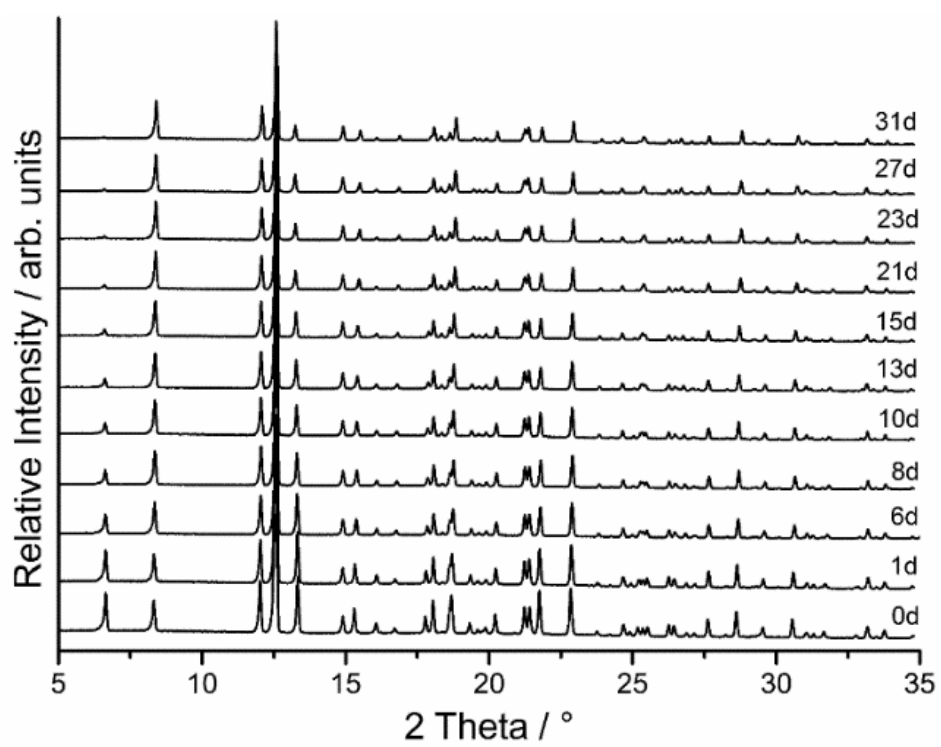


Figure S12. Time-dependent XRPD patterns of **1**-MeCN on storage at room-temperature.

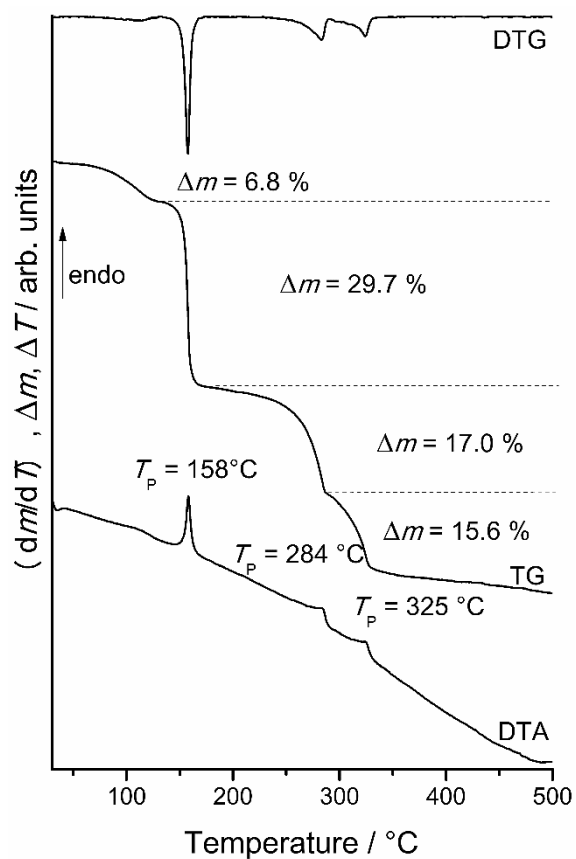


Figure S13. DTA-TG curve of **1** stored in an acetonitrile atmosphere for several hours.

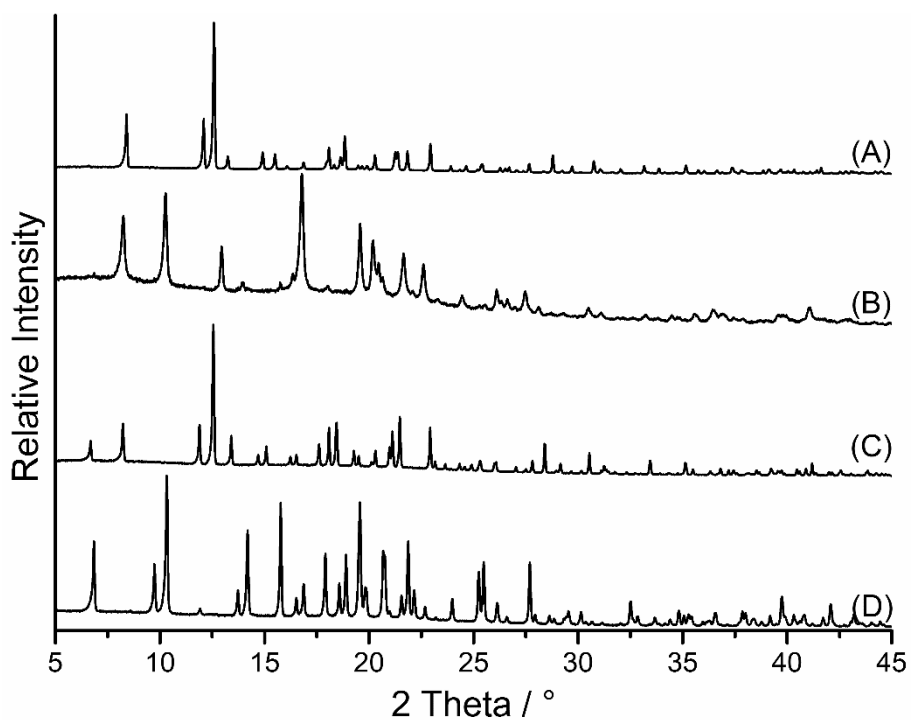


Figure S14. Experimental XRPD pattern of **1** (A) and XRPD patterns of **1** after one night in water (B) and ethanol (C) atmosphere as well as 1 h at a methanol atmosphere (D).

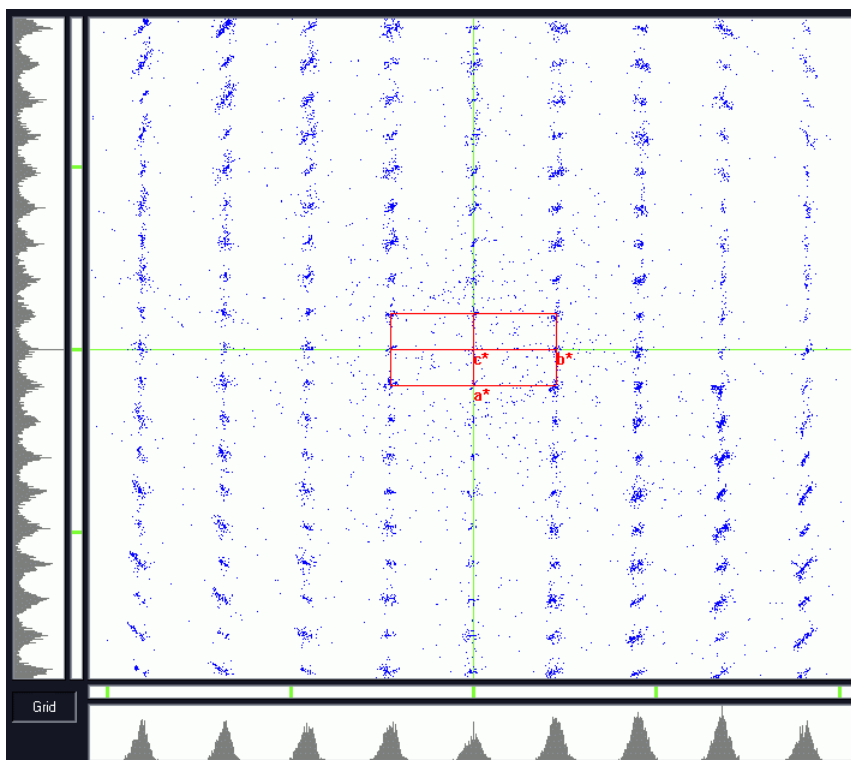
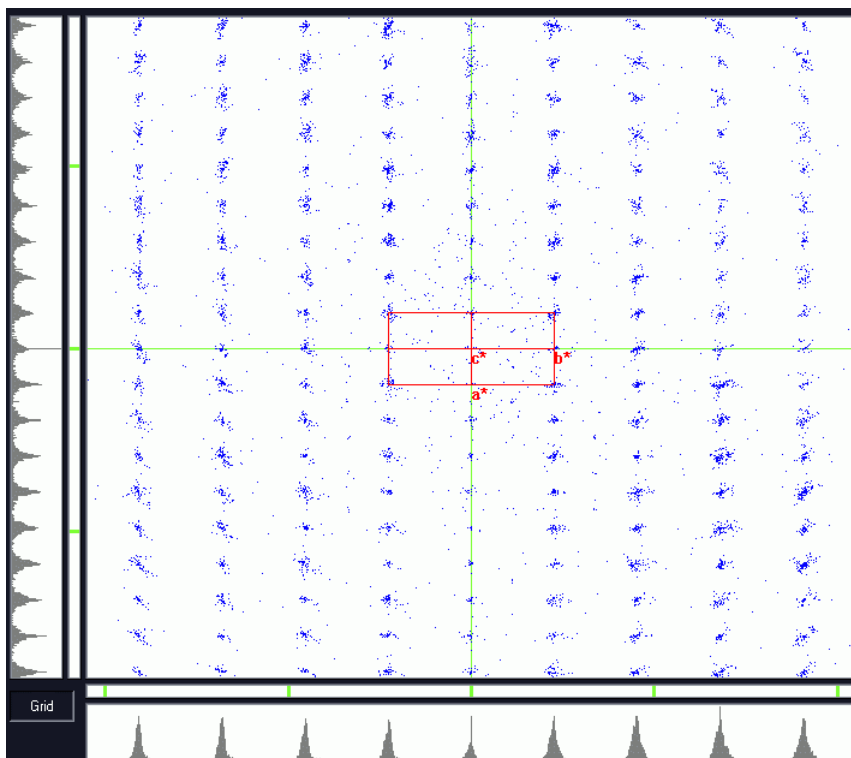


Figure S15. Reciprocal space plots for 1-MeCN (top) and 1-MeCN-A (bottom) with view along the c -axis. All peaks with $I \geq \sigma(I)$ are shown in yellow and information of the individual intensity of each reflection is lost.

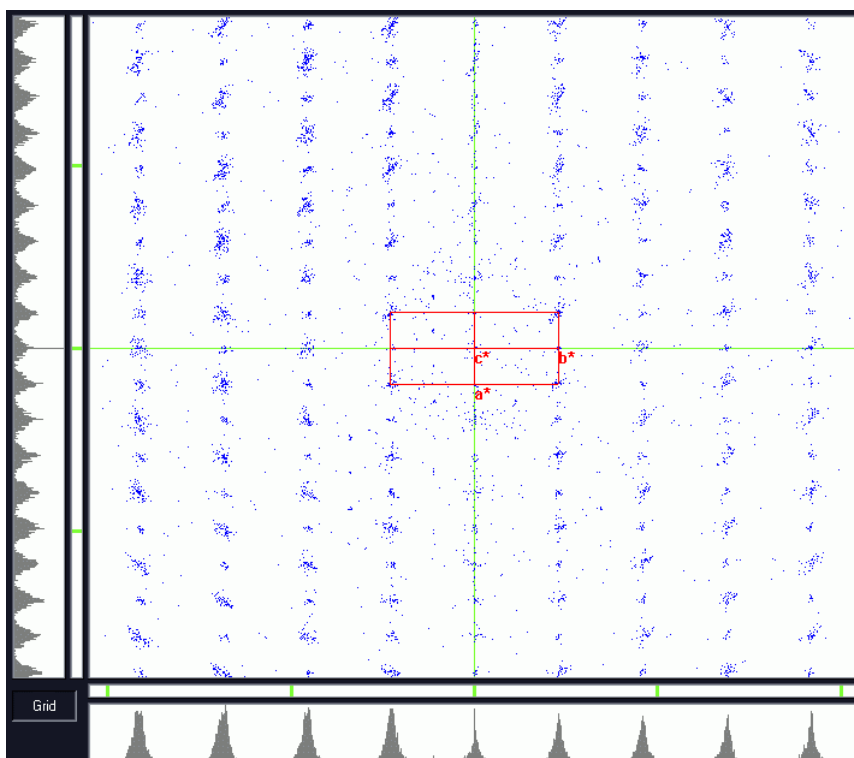
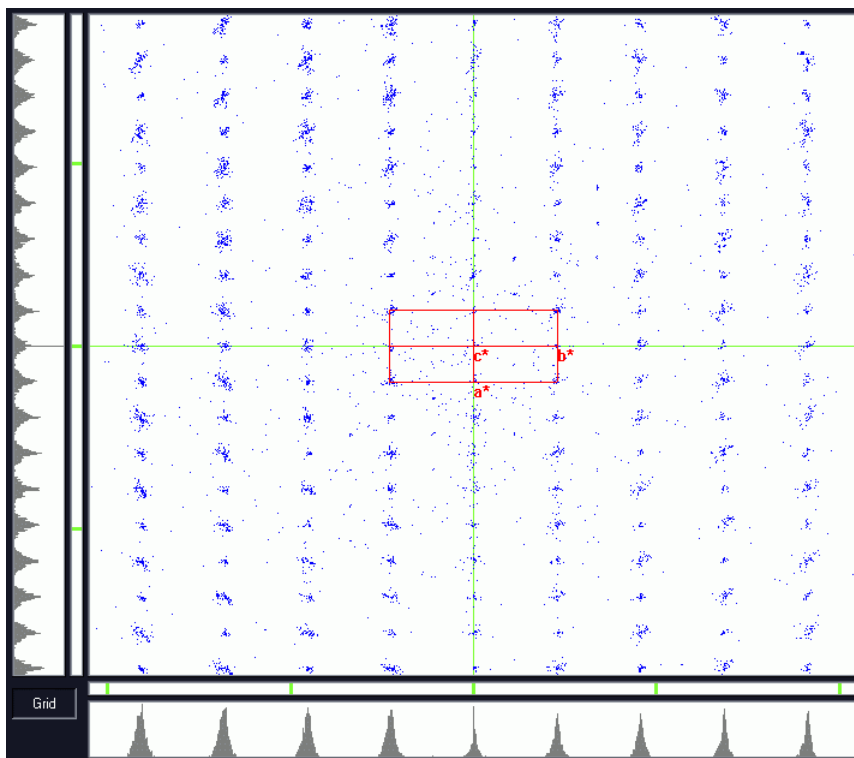


Figure S16. Reciprocal space plots for **1-MeCN-B** (top) and **1-MeCN-C** (bottom) with view along the c -axis. All peaks with $I \geq \sigma(I)$ are shown in yellow and information of the individual intensity of each reflection is lost.

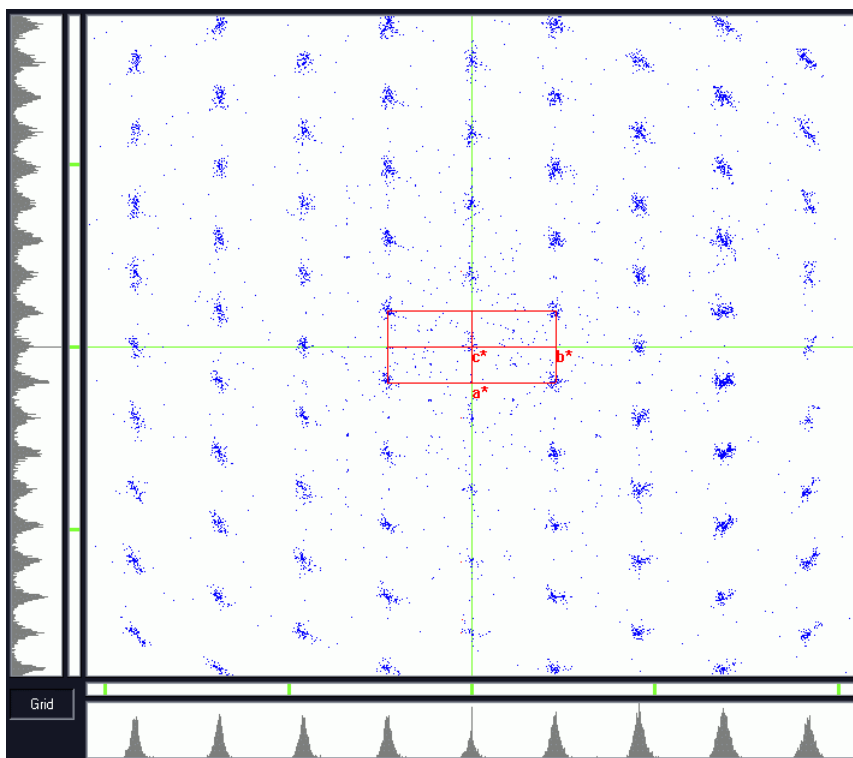
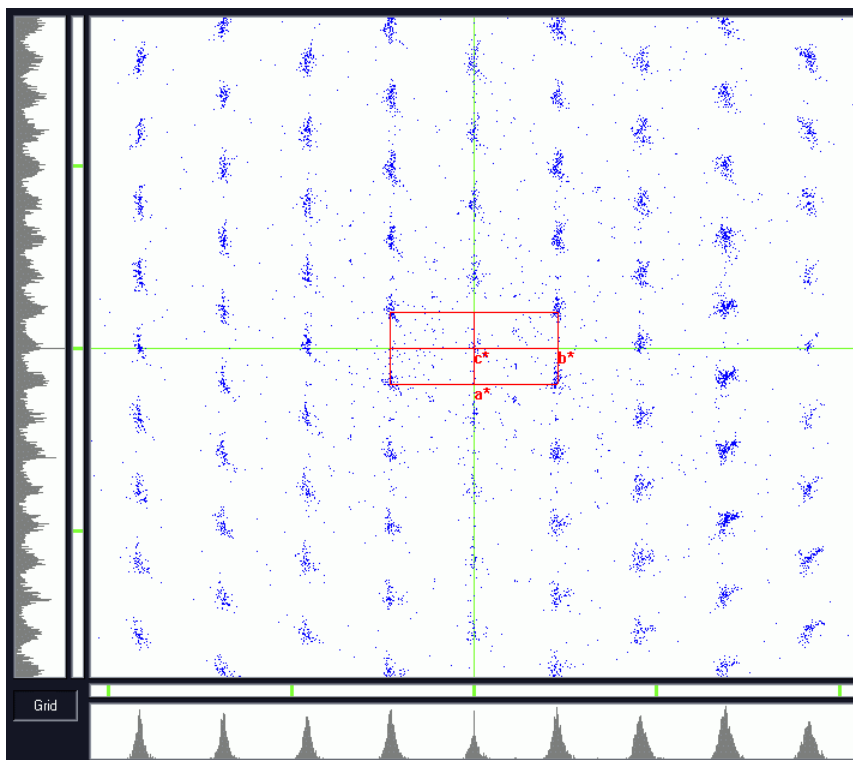


Figure S17. Reciprocal space plots for **1-MeCN-D** (top) and **1-MeCN-E** (bottom) with view along the c -axis. All peaks with $I \geq \sigma(I)$ are shown in yellow and information of the individual intensity of each reflection is lost.

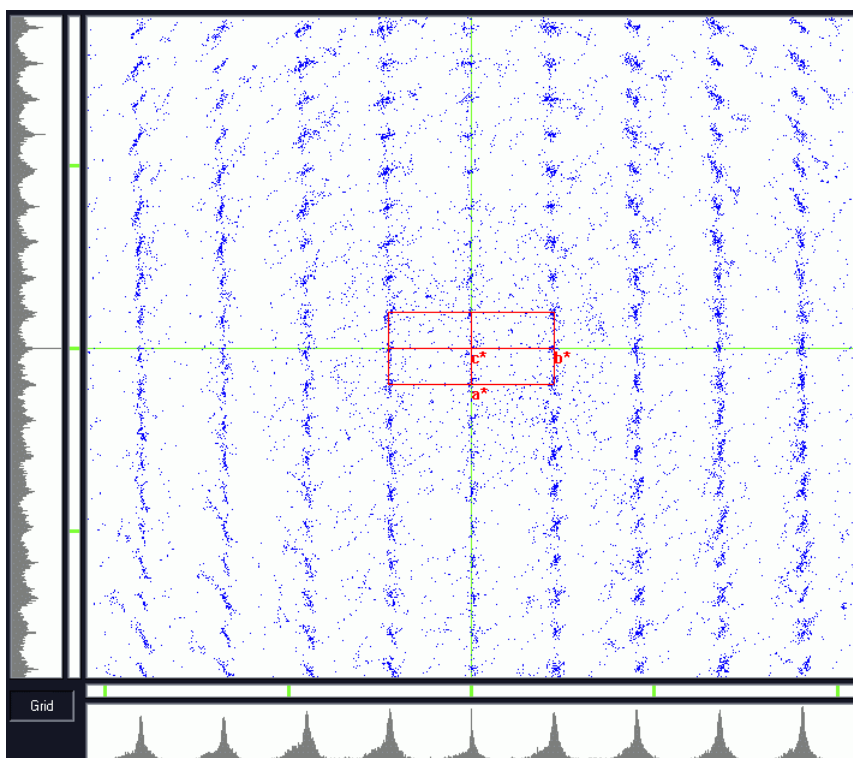
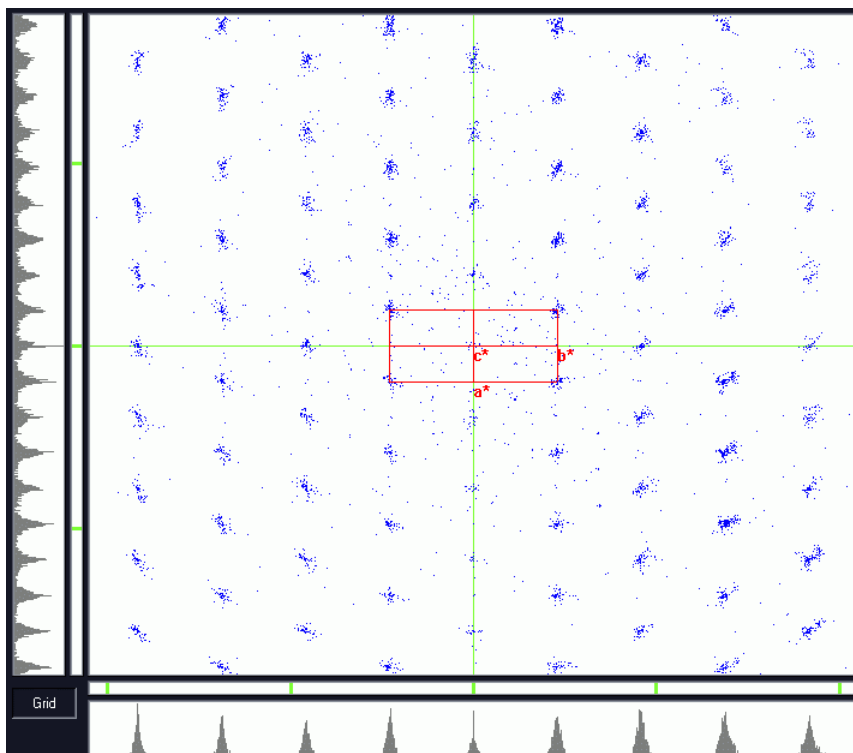


Figure S18. Reciprocal space plots for **1** (top) and **1-re** (bottom) with view along the c -axis. All peaks with $I \geq \sigma(I)$ are shown in yellow and information of the individual intensity of each reflection is lost.

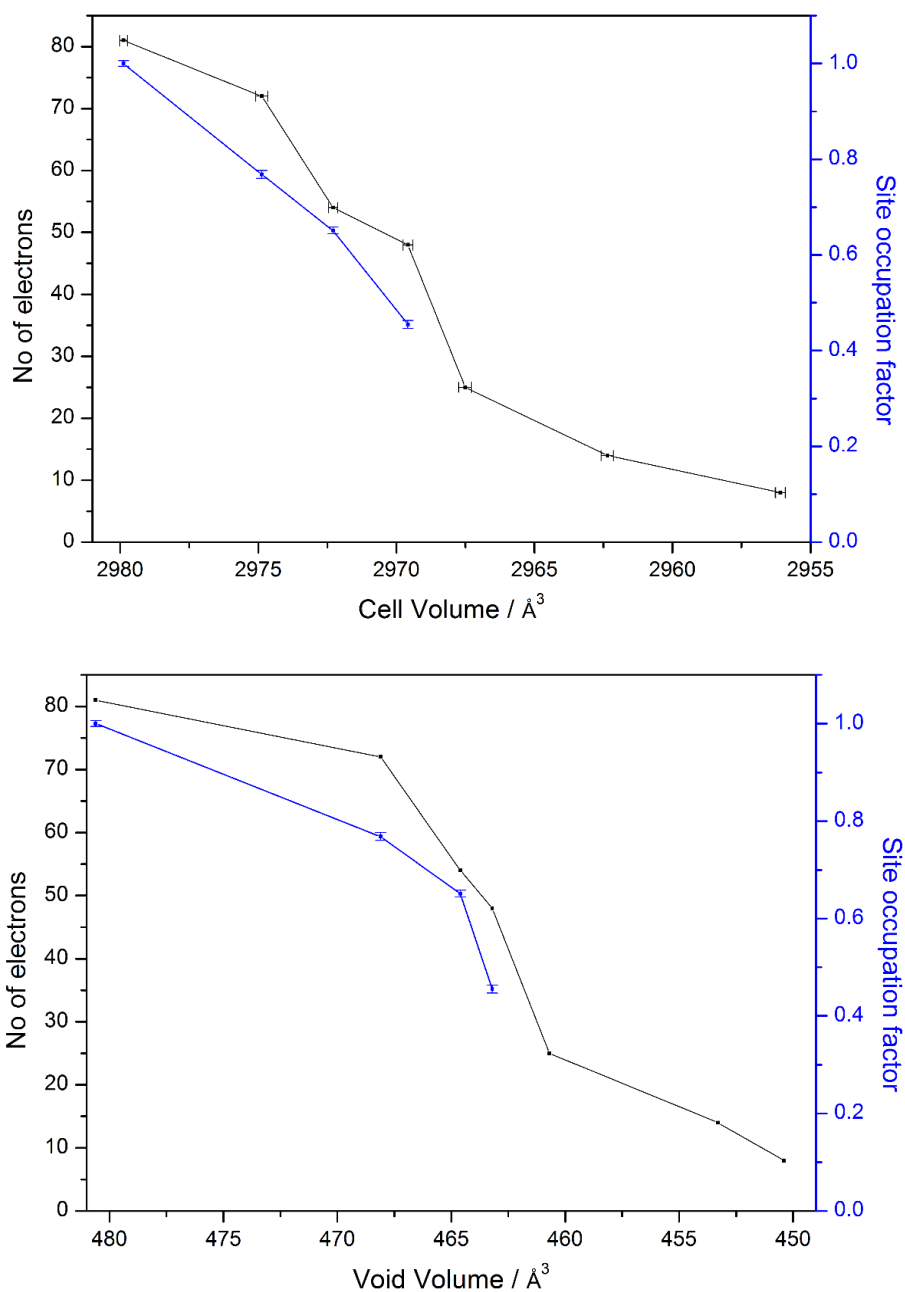


Figure S19. Unit cell (top) and void volume (bottom) as function of the number of electrons within the voids (black) and the site occupation factor (blue).

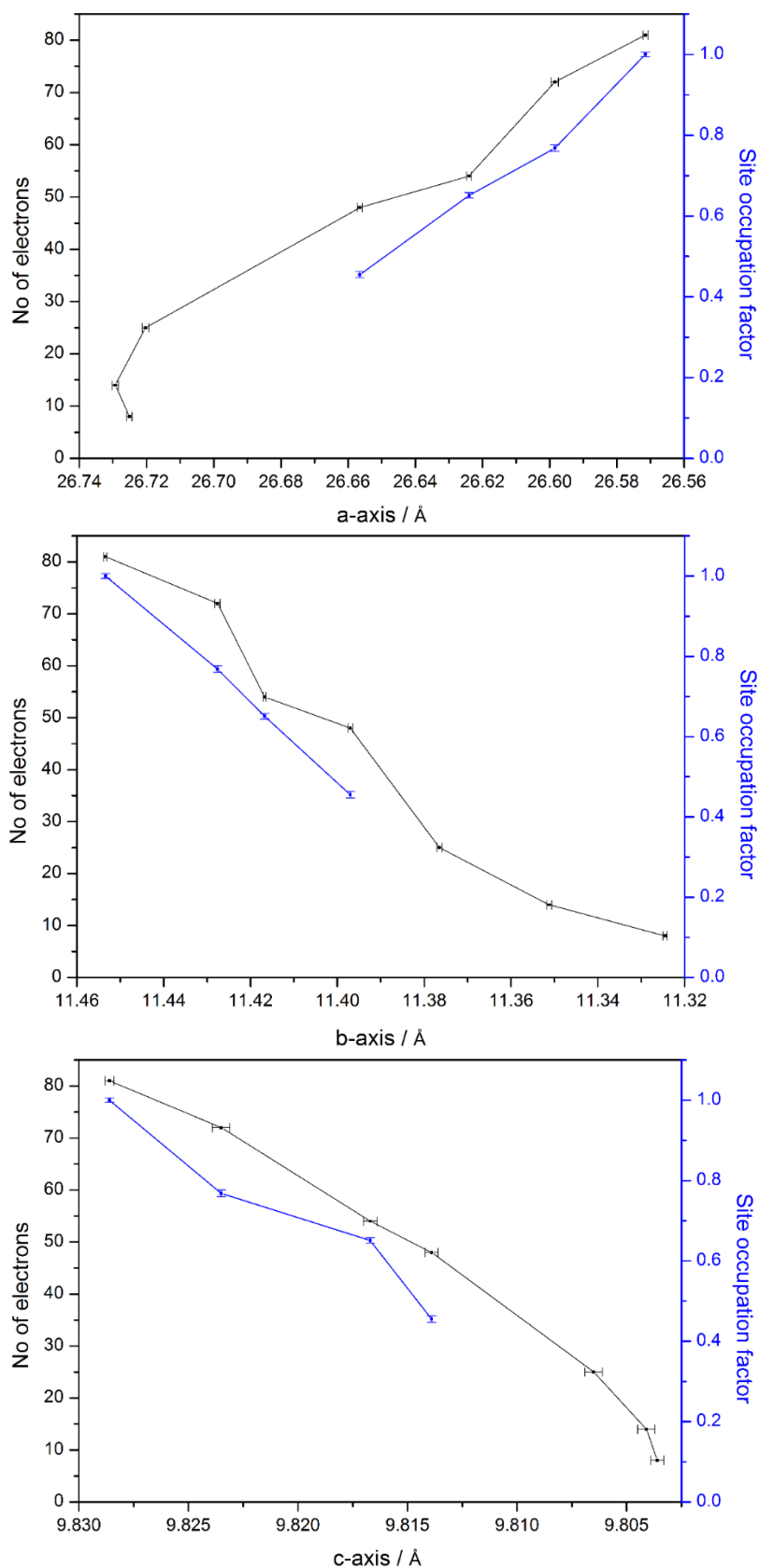


Figure S20. Length of the crystallographic *a*-, *b*- and *c*-axis as function of the number of electrons within the voids (black) and the site occupation factor (blue) of the acetonitrile molecules.

Table S4. Comparison of selected bond lengths and angles for **1**-MeCN and **1**.

1 -MeCN		1	
Ni(1)-N(2)	2.0306(17)	Ni(1)-N(1)	2.0300(17)
Ni(1)-N(1)	2.0334(17)	Ni(1)-N(1)#1	2.0299(17)
Ni(1)-N(11)	2.0968(16)	Ni(1)-N(11)	2.1054(15)
Ni(1)-N(21)	2.0986(16)	Ni(1)-N(11)#1	2.1054(15)
Ni(1)-S(2)#1	2.5417(5)	Ni(1)-S(1)#2	2.5362(5)
Ni(1)-S(1)#2	2.5595(5)	Ni(1)-S(1)#3	2.5362(5)
N(2)-Ni(1)-N(11)	90.33(6)	N(1)-Ni(1)-N(11)#1	90.18(6)
N(1)-Ni(1)-N(11)	92.05(6)	N(1)-Ni(1)-N(11)	91.64(6)
N(2)-Ni(1)-N(21)	91.44(6)	N(1)-Ni(1)-N(11)	91.64(6)
N(1)-Ni(1)-N(21)	90.53(6)	N(11)-Ni(1)-N(11)#1	90.25(8)
N(11)-Ni(1)-N(21)	90.86(7)	N(11)-Ni(1)-N(11)#1	90.25(8)
N(2)-Ni(1)-S(2)#1	85.25(5)	N(1)-Ni(1)-N(11)#1	90.18(6)
N(1)-Ni(1)-S(2)#1	92.72(4)	N(1)-Ni(1)-S(1)#3	92.82(4)
N(11)-Ni(1)-S(2)#1	90.48(4)	S(1)#2-Ni(1)-S(1)#3	88.63(3)
N(2)-Ni(1)-S(1)#2	92.08(4)	N(1)#1-Ni(1)-S(1)#2	92.82(4)
N(1)-Ni(1)-S(1)#2	85.50(5)	N(1)-Ni(1)-S(1)#2	85.33(5)
N(21)-Ni(1)-S(1)#2	90.36(5)	N(11)#1-Ni(1)-S(1)#2	90.64(4)
S(2)#1-Ni(1)-S(1)#2	88.45(2)	N(1)#1-Ni(1)-S(1)#3	85.33(5)
N(11)-Ni(1)-S(1)#2	177.28(4)	N(11)-Ni(1)-S(1)#2	176.84(4)
N(21)-Ni(1)-S(2)#1	176.44(4)	N(11)#1-Ni(1)-S(1)#3	176.84(4)
N(2)-Ni(1)-N(1)	176.89(7)	N(1)#1-Ni(1)-N(1)	177.43(8)

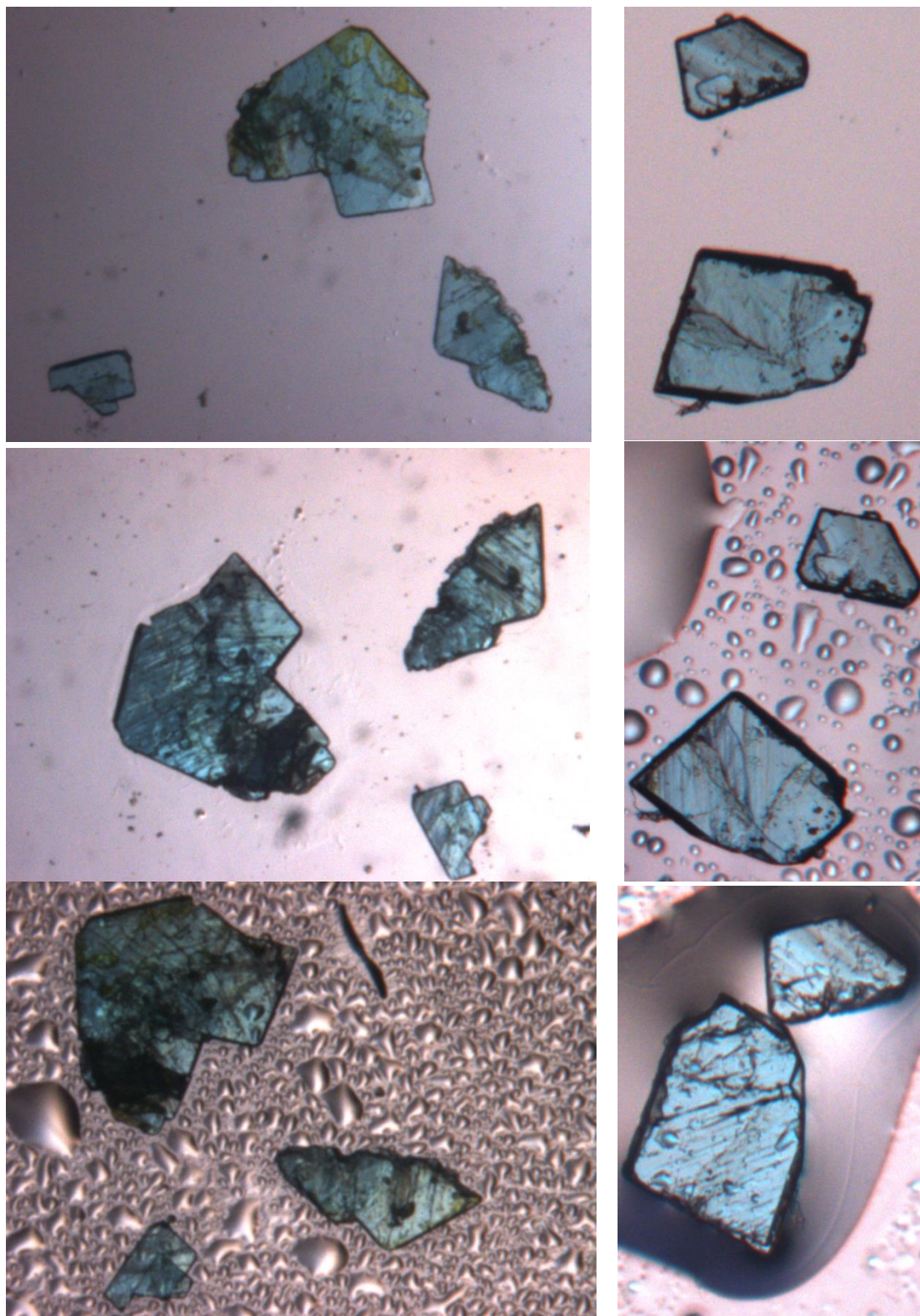


Figure S21. Microscopic images of selected crystals of **1-MeCN** (top), after removal of solvent (mid) and after storage in a saturated acetonitrile atmosphere (bottom).

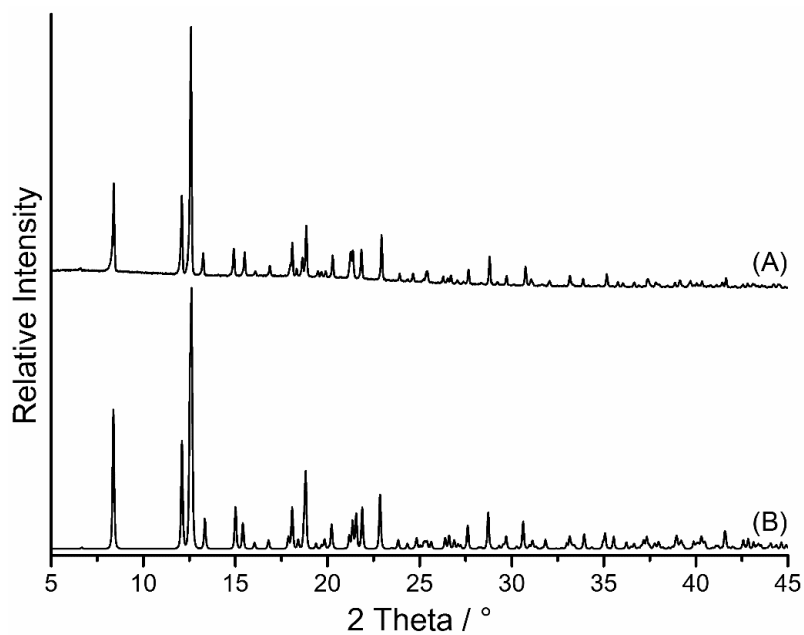


Fig. S22. Experimental XRPD pattern of **1** after sorption measurements (A) and calculated pattern of **1** (B).

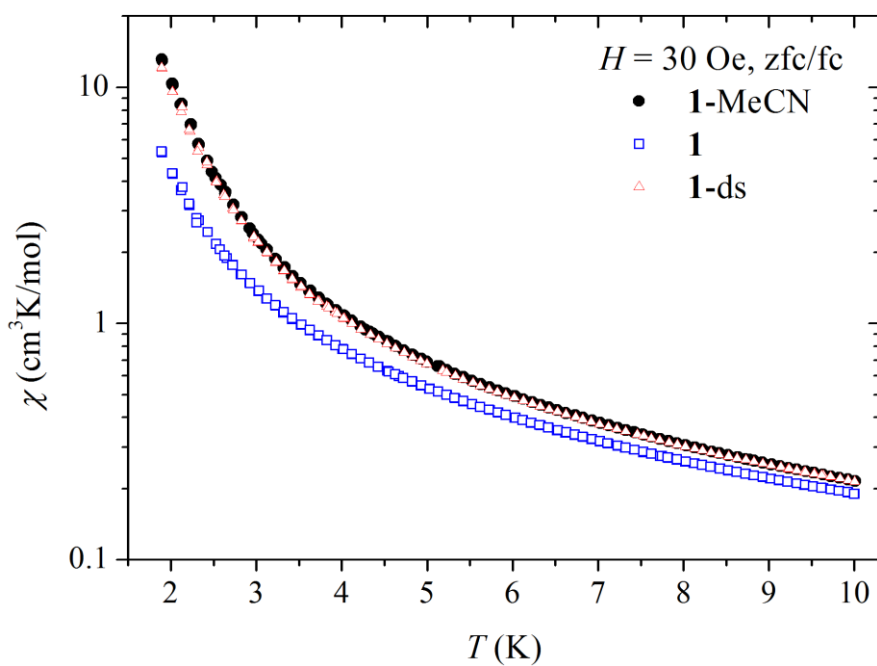


Fig S23. Magnetic susceptibility measured at 30 Oe for **1**-MeCN, **1** (dried sample) and **1ds** (sample dried and saturated again with MeCN). Zero-field cooling and field cooling modes of the measurement provide identical data.

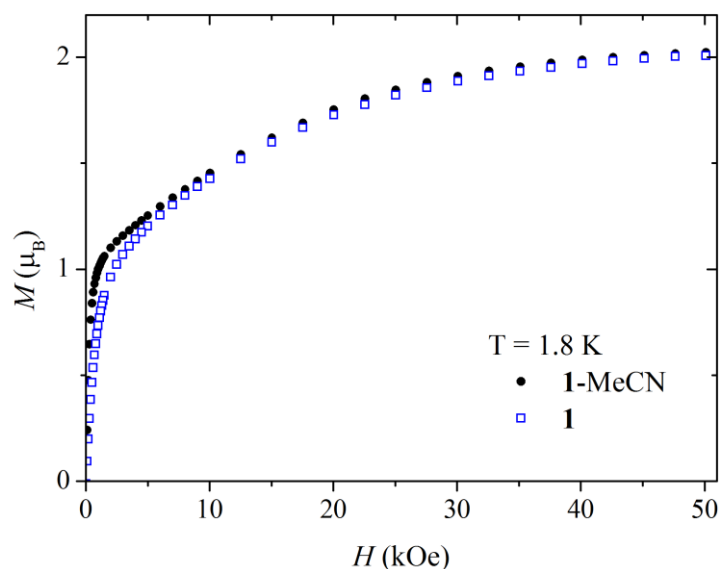


Figure S24. Field dependence of magnetization measured for **1**-MeCN (dots) and **1** (open squares) at 1.8 K.

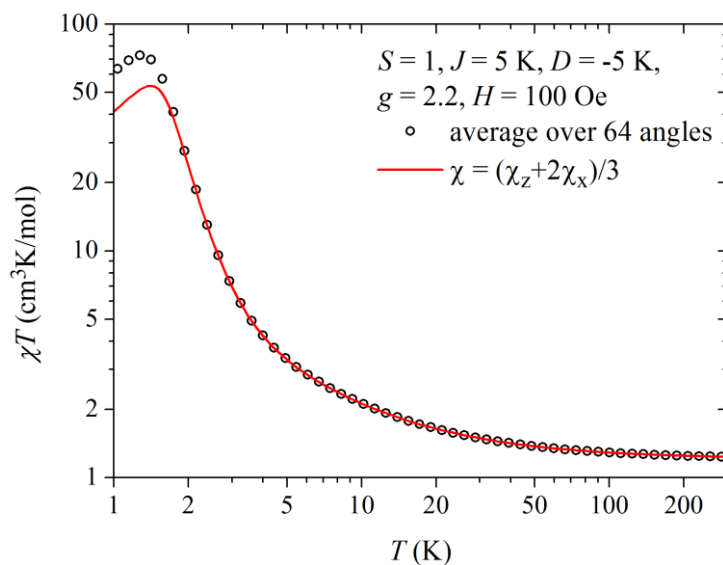


Figure S25. Comparison of two methods used to calculate susceptibility for a powder sample, which includes averaging susceptibility calculated for different directions of applied H field in respect to the z fs anisotropy axis. In the first method we used the average of susceptibility for 64 different angles between z axis and x axis with proper weights. In the second method the approximation $\chi = (2\chi_x + \chi_z)/3$ was used, which is much quicker to calculate. The latter method produces good results, unless the saturation of magnetization M is reached at very low temperatures, which influences χ calculated as M/H . The above simulation was made for $J = 5$ K and $D = -5$ K, $g = 2.2$, $H = 100$ Oe, i.e. parameters close to experimentally found for the presented compounds. The experimental data fulfill $\chi T < 30$ JmolK² at 100 Oe and are far from any influence of saturation by field. Thus, the $\chi = (2\chi_x + \chi_z)/3$ was used in all other calculations of low-field susceptibility.

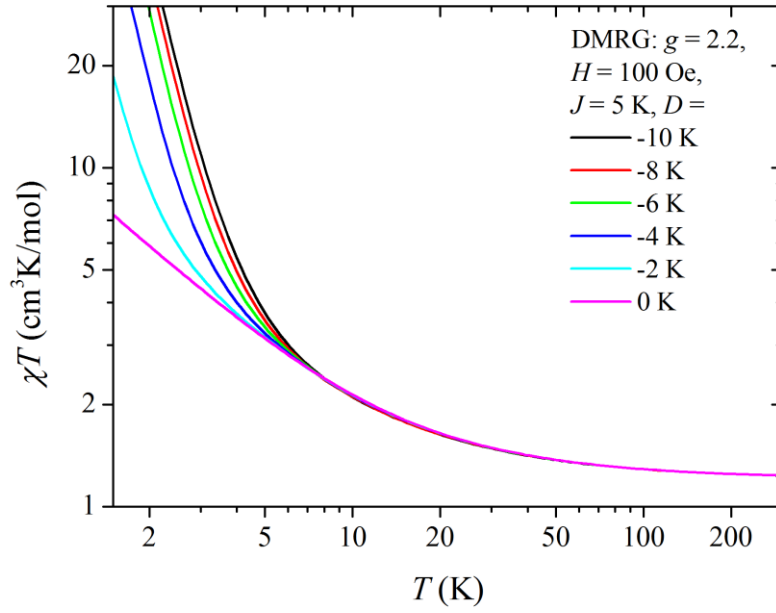


Figure S26. Magnetic susceptibility χ (powder average, shown χT product) calculated with DMRG method for the Heisenberg chain of spins $S = 1$ for different exchange interaction J and fixed zero-field splitting parameter D and fixed factor $g = 2.2$. The field $H = 100$ Oe is small enough to avoid any influence of χT saturation at low temperatures, in the range shown in the figure. Similar data (more dense) were used to calculate by scaling and by interpolation for other values of J , D and g for quick fitting of experimental data.

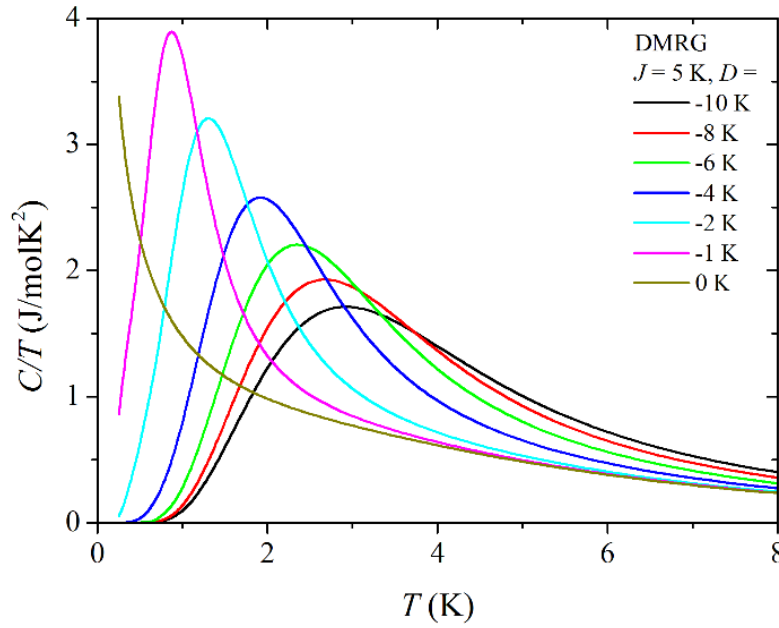


Figure S27. Specific heat C of the Heisenberg chain of spins $S = 1$ with fixed exchange interaction J and different zero-field splitting parameters D in zero field $H = 0$ calculated using the DMRG method. These results were used to fit the experimental results by scaling and interpolating.

Comments on the checkcif reports

If one look at the checkcif reports one will find for all structures refined in space group $P2_1/c$ that ADDSYM detects a potential lattice translation, which leads to space group $C2/c$. This is valid for 94% of all atoms in compound **1-MeCN** and to 100% to all other structures with less acetonitrile content. Consequently this one might take as a strong indication that space group $P2_1/c$ is at least for some structures wrong and that they might be better described in space group $C2/c$.

It is noted, that all structures including the acetonitrile solvate with full occupation of the acetonitrile atoms can be refined in $C2/c$, but in this case the solvent molecule is disordered in two orientations, whereas it is perfectly ordered in $P2_1/c$. In such cases there is no general rule which space group should be selected and in some cases it might be better to use the higher symmetry and to accept the small disorder. However, this would be acceptable if the rest of the structure would perfectly fulfill the C-centering but in this case one would expect large correlations between the parameters in the refinement in $P2_1/c$, but this is not the case here even if some of the solvent is removed.

The most important argument is the fact that a large amount of reflections are observed with $h+k = 2n+1$, which must be absent in space group $C2/c$. They are weak but they are clearly observed until some acetonitrile content. These reflections are truth and cannot be traced back to, e.g., $\lambda/2$ effect, which can happen if an area detector without energy discrimination is used.

Because the intensity of these reflections decreases with decreasing acetonitrile content, the transition is smeared and it is difficult to decide when the refinement in $C2/c$ might be more appropriate. Therefore, at some composition it might be a matter of taste, which space group might be more appropriate.

However, in our case we have refined all structures in $P2_1/c$, for which the super structure reflections are clearly visible (see figures S15-S18) and in which the site occupation factor of the acetonitrile atoms can be refined to reasonable and significant values.

That the description in $P2_1/c$ is correct for **1-MeCN** is obvious from the fact, that the higher symmetry is valid to only 94% of the structures. Surprisingly for all refinements in $P2_1/c$, in which the sof of the solvent molecules is below 1, in the checkcif report it is mentioned that the higher symmetry is valid for 100% of all atoms but this is clearly wrong. A closer look on the adsymm output reveals, that in this case the acetonitrile atoms are not considered in the symmetry check, which is surprising. Therefore, it must lead to a fit of 100% but this is definitely not correct and one must also kept in mind, that the intensities of the reflections are not considered by this program.

Summarizing, we are sure that the choice of the space group was made correctly but it is also clear that the exact composition where the lattice symmetry changes cannot be determined very precisely. The latter is not of importance for the overall story.